Hindawi Publishing Corporation
Mathematical Problems in Engineering
Volume 2013, Article ID 831725, 10 pages
http://dx.doi.org/10.1155/2013/831725

Research Article

Numerical Investigation of the Effect of Magnetic Field on Natural Convection in a Curved-Shape Enclosure

M. Sheikholeslami,[1] I. Hashim,[2] and Soheil Soleimani[3]

[1] *Department of Mechanical Engineering, Babol University of Technology, 484 Babol, Iran*
[2] *Solar Energy Research Institute, Universiti Kebangsaan Malaysia, 43600 Bangi, Selangor, Malaysia*
[3] *Department of Mechanical and Materials Engineering, Florida International University, Miami, FL 33199, USA*

Correspondence should be addressed to I. Hashim; ishak_h@ukm.my

Received 30 January 2013; Accepted 29 March 2013

Academic Editor: Kuppalapalle Vajravelu

This investigation reports the magnetic field effect on natural convection heat transfer in a curved-shape enclosure. The numerical investigation is carried out using the control volume-based-finite element method (CVFEM). The numerical investigations are performed for various values of Hartmann number and Rayleigh number. The obtained results are depicted in terms of streamlines and isotherms which show the significant effects of Hartmann number on the fluid flow and temperature distribution inside the enclosure. Also, it was found that the Nusselt number decreases with an increase in the Hartmann number.

1. Introduction

The study of natural convection in horizontal annuli is of importance in many industrial and geophysical problems. This topic is of practical interest in several applications such as solar collector-receiver, underground electric transmission cables, vapor condenser for water distillation, and food processing. Mohammed et al. [1] experimentally investigated the forced and free convection for thermally developing and fully developed laminar airflow inside a horizontal concentric annulus. They showed that the Nusselt number is considerably greater for developing flow than the corresponding values for fully developed flow over a significant portion of the annulus. Kuehn and Goldstein [2] presented experimental and numerical studies of steady-state natural convection heat transfer in a horizontal concentric annulus. They studied parametrically the effects of the Rayleigh and Prandtl numbers and aspect ratio and proposed correlating equations. Natural convection between a square outer cylinder and a heated elliptic inner cylinder was studied numerically by Bararnia et al. [3]. They found that streamlines and isotherms strongly depend on the Rayleigh number and the position of the inner cylinder. Recently, several papers were published about natural convection [4–13].

Natural convection under the influence of a magnetic field is of great importance in many industrial applications such as crystal growth in liquid, cooling of nuclear reactor, electronic package, microelectronic devices, and solar technology. In the case of free convection of an electrically conducting fluid in the presence of a magnetic field, there are two body forces: buoyancy force and Lorentz force. They interact with each other and can influence heat and mass transfer. Thus, it is important to study the detailed characteristics of transport phenomena in such a process to have a better product with improved design. Magnetohydrodynamic natural convection in a vertical cylindrical cavity with a sinusoidal upper wall temperature was investigated by Kakarantzas et al. [14]. They concluded that the increase of Hartmann number results in a damping of the fluid motion, and thus heat conduction progressively dominates over convection heat transfer. Rudraiah et al. [15] investigated numerically the effect of a magnetic field on natural convection in a rectangular enclosure. They found that the magnetic field decreases the rate of heat transfer. Sheikholeslami et al. [16] studied the natural convection in a concentric annulus between a cold outer square and heated inner circular cylinders in the presence of a static radial magnetic field. They reported that the average Nusselt number is an increasing function

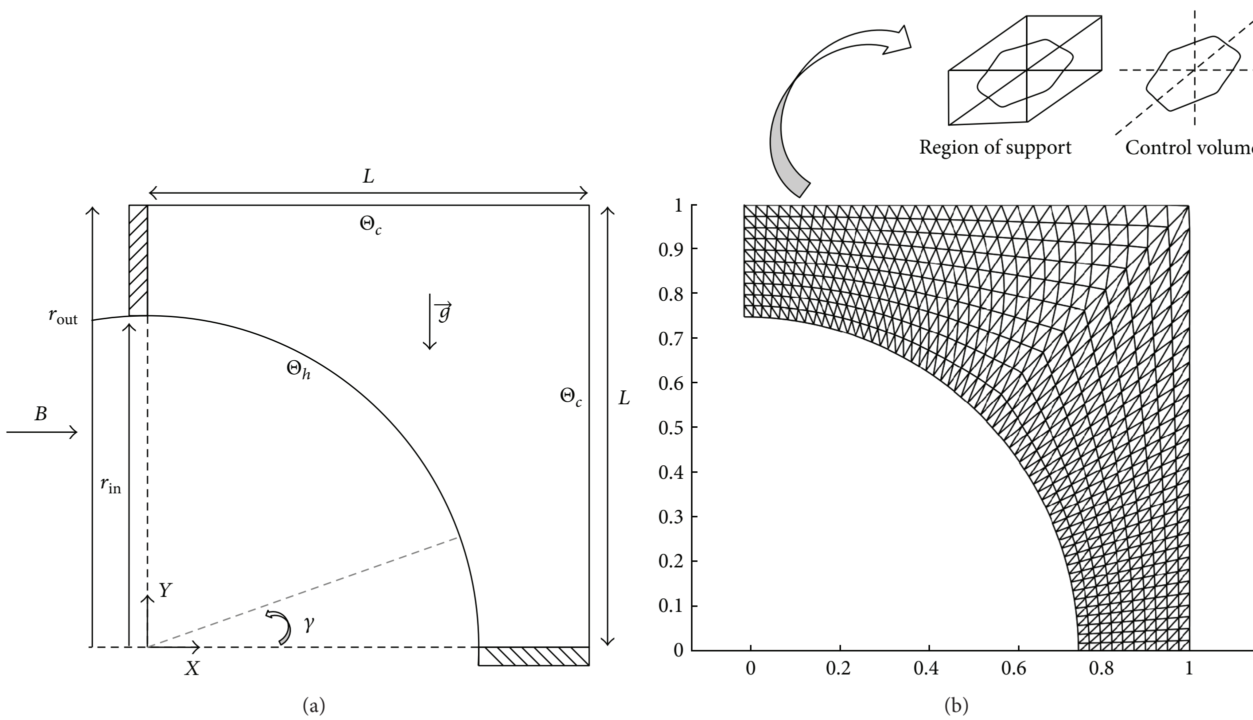

FIGURE 1: (a) Geometry and the boundary conditions with (b) the mesh of enclosure considered in this work.

of the nanoparticle volume fraction parameter and Rayleigh number, while it is a decreasing function of Hartmann number. Effect of magnetic field on natural convection was considered by several authors [17–29].

Control volume-based-finite-element method (CVFEM) is a scheme that uses the advantages of both finite-volume and finite-element methods for simulation of multiphysics problems in complex geometries [30, 31]. Soleimani et al. [32] studied natural convection heat transfer in a semiannulus enclosure filled with nanofluid using CVFEM. They found that the angle of turn has an important effect on the streamlines, isotherms, and maximum or minimum values of the local Nusselt number. Sheikholeslami et al. [33] performed a numerical analysis for natural convection heat transfer of Cu-water nanofluid in a cold outer circular enclosure containing a hot inner sinusoidal circular cylinder in the presence of a horizontal magnetic field using CVFEM. They concluded that in the absence of a magnetic field, the enhancement ratio decreases as the Rayleigh number increases, while an opposite trend is observed in the presence of a magnetic field. Also, they found that the average Nusselt number is an increasing function of the nanoparticle volume fraction parameter, the number of undulations, and Rayleigh number, while it is a decreasing function of the Hartmann number. The applications of this method were introduced by different authors [34, 35].

The main goal of the present work is to conduct a numerical investigation of natural convection heat transfer in a curved-shape enclosure in the presence of a magnetic field using CVFEM. The numerical investigation is carried out for different values of the governing parameters.

2. Problem Formulation

The physical model along with the important geometrical parameters is shown in Figure 1(a). The width and height of the enclosure is H. The right and top walls of the enclosure are maintained at constant cold temperature T_c, whereas the inner circular hot wall is maintained at constant hot temperature T_h and the bottom and left walls with the length of $H/2$ are thermally insulated. Under all cases, $T_h > T_c$ condition is maintained.

To assess the shape of inner circular and outer rectangular boundaries which consist of the right and top walls, an elliptic function can be used as follows:

$$\left(\frac{X}{a}\right)^{2\hat{n}} + \left(\frac{Y}{b}\right)^{2\hat{n}} = 1. \quad (1)$$

When $a = b$ and $\hat{n} = 1$, the geometry becomes a circle. As $\hat{n}$ increases from 1, the geometry would approach a rectangle for $a \neq b$ and square for $a = b$. It is also assumed that the uniform magnetic field ($\vec{B} = B_x\vec{e_x} + B_y\vec{e_y}$) of constant magnitude $B = \sqrt{B_x^2 + B_y^2}$ is applied, where $\vec{e_x}$ and $\vec{e_y}$ are unit vectors in the Cartesian coordinate system. The orientation of the magnetic field forms an angle γ with horizontal axis such that $\gamma = B_x/B_y$. The electric current J and the electromagnetic force F are defined by $J = \sigma(\vec{V} \times \vec{B})$ and $F = \sigma(\vec{V} \times \vec{B}) \times \vec{B}$, respectively.

The flow is two-dimensional, laminar, and incompressible. The radiation, viscous dissipation, induced electric current, and Joule heating are neglected. The magnetic Reynolds number is assumed to be small so that the induced magnetic field can be neglected compared to the applied magnetic field. Now using the Boussinesq approximation, the governing equations can be obtained in dimensional form as follows [15]:

$$\frac{\partial u}{\partial x}+\frac{\partial v}{\partial y}=0, \tag{2}$$

$$\begin{aligned} u\frac{\partial u}{\partial x}+v\frac{\partial u}{\partial y} &= -\frac{1}{\rho}\frac{\partial P}{\partial x}+\upsilon\left(\frac{\partial^2 u}{\partial x^2}+\frac{\partial^2 u}{\partial y^2}\right) \\ &\quad+\frac{\sigma B^2}{\rho}\left(v\sin\lambda\cos\lambda-u\sin^2\lambda\right), \end{aligned} \tag{3}$$

$$\begin{aligned} u\frac{\partial v}{\partial x}+v\frac{\partial v}{\partial y} &= -\frac{1}{\rho}\frac{\partial P}{\partial y}+\upsilon\left(\frac{\partial^2 v}{\partial x^2}+\frac{\partial^2 v}{\partial y^2}\right)+\beta g\left(T-T_c\right) \\ &\quad+\frac{\sigma B^2}{\rho}\left(u\sin\lambda\cos\lambda-v\cos^2\lambda\right), \end{aligned} \tag{4}$$

$$u\frac{\partial T}{\partial x}+v\frac{\partial T}{\partial y}=\alpha\left(\frac{\partial^2 T}{\partial x^2}+\frac{\partial^2 T}{\partial y^2}\right). \tag{5}$$

The stream function and vorticity are defined as follows:

$$u=\frac{\partial\psi}{\partial y},\qquad v=-\frac{\partial\psi}{\partial x},\qquad \omega=\frac{\partial v}{\partial x}-\frac{\partial u}{\partial y}. \tag{6}$$

The stream function satisfies the continuity equation (2). The vorticity equation is obtained by eliminating the pressure between the two momentum equations, that is, by taking the y-derivative of (3) and subtracting from it the x-derivative of (4). This gives

$$\begin{aligned} &\frac{\partial\psi}{\partial y}\frac{\partial\omega}{\partial x}-\frac{\partial\psi}{\partial x}\frac{\partial\omega}{\partial y} \\ &\quad=\upsilon\left(\frac{\partial^2\omega}{\partial x^2}+\frac{\partial^2\omega}{\partial y^2}\right)+\beta g\left(\frac{\partial T}{\partial x}\right) \\ &\qquad+\frac{\sigma B^2}{\rho}\left(-\frac{\partial v}{\partial y}\sin\lambda\cos\lambda+\frac{\partial u}{\partial y}\sin^2\lambda\right. \\ &\qquad\qquad\left.+\frac{\partial u}{\partial x}\sin\lambda\cos\lambda-\frac{\partial v}{\partial x}\cos^2\lambda\right), \\ &\frac{\partial\psi}{\partial y}\frac{\partial T}{\partial x}-\frac{\partial\psi}{\partial x}\frac{\partial T}{\partial y}=\alpha\left(\frac{\partial^2 T}{\partial x^2}+\frac{\partial^2 T}{\partial y^2}\right), \\ &\frac{\partial^2\psi}{\partial x^2}+\frac{\partial^2\psi}{\partial y^2}=-\omega. \end{aligned} \tag{7}$$

Nondimensional variables are defined as follows:

$$\begin{aligned} &X=\frac{x}{L},\qquad Y=\frac{y}{L},\qquad \Omega=\frac{\omega L^2}{\alpha},\qquad \Psi=\frac{\psi}{\alpha}, \\ &\Theta=\frac{T-T_c}{T_h-T_c},\qquad U=\frac{\nu L}{\alpha},\qquad V=\frac{\nu L}{\alpha}, \end{aligned} \tag{8}$$

where $L=r_{\text{out}}-r_{\text{in}}=r_{\text{in}}$. Using the dimensionless parameters, the equations now become as follows:

$$\begin{aligned} &\frac{\partial\Psi}{\partial Y}\frac{\partial\Omega}{\partial X}-\frac{\partial\Psi}{\partial X}\frac{\partial\Omega}{\partial Y} \\ &\quad=\Pr\left(\frac{\partial^2\Omega}{\partial X^2}+\frac{\partial^2\Omega}{\partial Y^2}\right)+\mathrm{Ra}\Pr\left(\frac{\partial\Theta}{\partial X}\right)+\mathrm{Ha}^2\Pr \\ &\qquad\times\left(-\frac{\partial V}{\partial Y}\tan\lambda+\frac{\partial U}{\partial Y}\tan^2\lambda+\frac{\partial U}{\partial X}\tan\lambda-\frac{\partial V}{\partial X}\right), \\ &\frac{\partial\Psi}{\partial Y}\frac{\partial\Theta}{\partial X}-\frac{\partial\Psi}{\partial X}\frac{\partial\Theta}{\partial Y}=\left(\frac{\partial^2\Theta}{\partial X^2}+\frac{\partial^2\Theta}{\partial Y^2}\right), \\ &\frac{\partial^2\Psi}{\partial X^2}+\frac{\partial^2\Psi}{\partial Y^2}=-\Omega, \end{aligned} \tag{9}$$

where $\mathrm{Ra}=g\beta L^3(T_h-T_c)/(\alpha\upsilon)$ is the Rayleigh number, $\mathrm{Ha}=LB_x\sqrt{\sigma/\mu}$ is the Hartmann number, and $\Pr=\upsilon/\alpha$ is the Prandtl number. The boundary conditions as shown in Figure 1 are

$$\begin{aligned} &\Theta=1.0 \text{ on the inner circular boundary}, \\ &\Theta=0.0 \text{ on the outer circular boundary}, \\ &\frac{\partial\Theta}{\partial n}=0.0 \text{ on the two other insulation boundaries}, \\ &\Psi=0.0 \text{ on all solid boundaries}. \end{aligned} \tag{10}$$

The values of vorticity on the boundary of the enclosure can be obtained using the stream function formulation and the known velocity conditions during the iterative solution procedure. The local Nusselt number along the hot wall can be expressed as

$$\mathrm{Nu}_{\text{loc}}=\left.\frac{\partial\Theta}{\partial n}\right|_{\text{hot wall}}, \tag{11}$$

where n is the direction normal to the inner circular wall. The average Nusselt number on hot wall is evaluated as

$$\mathrm{Nu}_{\text{ave}}=\frac{1}{\pi/2}\int_0^{\pi/2}\mathrm{Nu}_{\text{local}}(\theta)\,d\theta. \tag{12}$$

3. Numerical Procedure

The mesh of the enclosure used in the present CVFEM program is shown in Figure 1(b). Triangular elements are considered as the building block of the discretization using CVFEM. The values of variables are approximated with linear interpolation within each element. A control volume is created by joining the center of each element in the support to the midpoints of the element sides that pass through the central node i, which creates a close polygonal control volume (see Figure 1(b)). To illustrate the solution procedure using the CVFEM, one can consider the general form of advection-diffusion equation for node i in integral form

$$-\int_V Q\,dV-\int_A k\nabla\phi\cdot n\,dA+\int_A(v\cdot n)\,\phi\,dA=0 \tag{13}$$

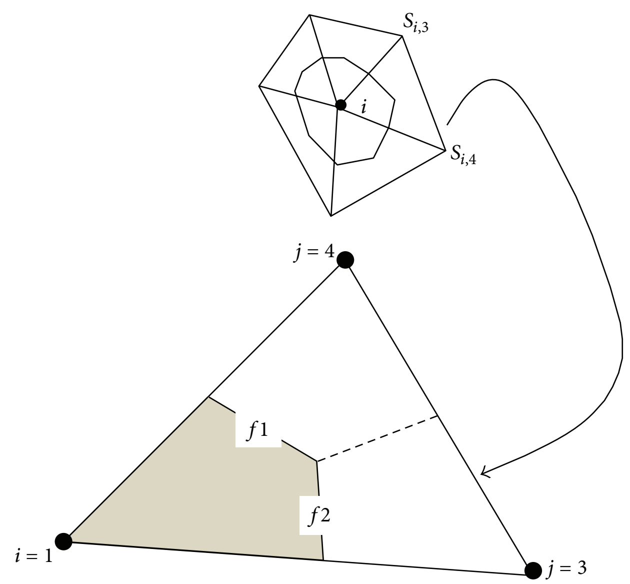

Figure 2: A sample triangular element and its corresponding control volume.

or point form

$$-\nabla \cdot (k \nabla \phi) + \nabla \cdot (v\phi) - Q = 0, \tag{14}$$

which can be represented by the system of CVFEM discrete equations as

$$\left[a_i + Qc_i + Bc_i\right] \phi_i = \sum_{j=1}^{n_i} a_{i,j}\, \phi_{S_{i,j}} + Q_{B_i} + B_{B_i}. \tag{15}$$

In the aforementioned, the a's are the coefficients, the index (i, j) indicates the jth node in the support of node i, the index $S_{i,j}$ provides the node number of the jth node in the support, the B's account for boundary conditions, and the Q's account for source terms. For the selected triangular element which is shown in Figure 2, the approximation without considering the source terms leads to

$$-\left(a_1^k + a_1^u\right) \phi_i + \left(a_2^k + a_2^u\right) \phi_{S_{i,3}} + \left(a_2^k + a_2^u\right) \phi_{S_{i,4}} = 0. \tag{16}$$

Using upwinding, the advective coefficients identified with the superscripts $()^u$ are given by

$$\begin{aligned} a_1^u &= \max\left[q_{f1}, 0\right] + \max\left[q_{f2}, 0\right], \\ a_2^u &= \max\left[-q_{f1}, 0\right], \\ a_3^u &= \max\left[-q_{f2}, 0\right], \end{aligned} \tag{17}$$

and the diffusion coefficients, identified with the superscripts $()^k$, are given by

$$\begin{aligned} a_1^k =& - k_{f1} N_{1x} \Delta\vec{y}_{f1} + k_{f1} N_{1y} \Delta\vec{x}_{f1} - k_{f2} N_{1x} \Delta\vec{y}_{f2} \\ & + k_{f2} N_{1y} \Delta\vec{x}_{f2}, \\ a_2^k =& - k_{f1} N_{2x} \Delta\vec{y}_{f1} + k_{f1} N_{2y} \Delta\vec{x}_{f1} - k_{f2} N_{2x} \Delta\vec{y}_{f2} \\ & + k_{f2} N_{2y} \Delta\vec{x}_{f2}, \\ a_2^k =& - k_{f1} N_{3x} \Delta\vec{y}_{f1} + k_{f1} N_{3y} \Delta\vec{x}_{f1} - k_{f2} N_{3x} \Delta\vec{y}_{f2} \\ & + k_{f2} N_{3y} \Delta\vec{x}_{f2}. \end{aligned} \tag{18}$$

In (17), the volume flow across faces 1 and 2 in the direction of the outward normal is

$$\begin{aligned} q_{f1} &= v \cdot n\, A|_{f1} = v_x^{f1} \Delta\vec{y}_{f1} - v_y^{f1} \Delta\vec{y}_{f1}, \\ q_{f2} &= v \cdot n\, A|_{f2} = v_x^{f2} \Delta\vec{y}_{f2} - v_y^{f2} \Delta\vec{y}_{f2}. \end{aligned} \tag{19}$$

The value of the diffusivity at the midpoint of face 1 is

$$k_{f1} = \left[N_1 k_1 + N_2 k_2 + N_3 k_3\right]_{f1} = \frac{5}{12} k_1 + \frac{5}{12} k_2 + \frac{2}{12} k_3 \tag{20}$$

and at the midpoint of face 2 is

$$k_{f2} = \left[N_1 k_1 + N_2 k_2 + N_3 k_3\right]_{f2} = \frac{5}{12} k_1 + \frac{2}{12} k_2 + \frac{5}{12} k_3. \tag{21}$$

The velocity components at the midpoint of face 1 are

$$\begin{aligned} v_x^{f1} &= \frac{5}{12} v_{x_1} + \frac{5}{12} v_{x_2} + \frac{2}{12} v_{x_3} \\ v_y^{f1} &= \frac{5}{12} v_{y_1} + \frac{5}{12} v_{y_2} + \frac{2}{12} v_{y_3} \end{aligned} \tag{22}$$

and on face 2 are

$$\begin{aligned} v_x^{f2} &= \frac{5}{12} v_{x_1} + \frac{2}{12} v_{x_2} + \frac{5}{12} v_{x_3}, \\ v_y^{f2} &= \frac{5}{12} v_{y_1} + \frac{2}{12} v_{y_2} + \frac{5}{12} v_{y_3}. \end{aligned} \tag{23}$$

These values can be used to update the ith support coefficients through the following equations:

$$\begin{aligned} a_i &= a_i + a_1^k, \\ a_{i,3} &= a_{i,3} + a_2^k, \\ a_{i,4} &= a_{i,4} + a_3^k. \end{aligned} \tag{24}$$

In (18), moving counterclockwise around node i, the signed distances are

$$\begin{aligned} \Delta\vec{x}_{f1} &= \frac{x_3}{3} - \frac{x_2}{6} - \frac{x_1}{6}, \qquad \Delta\vec{x}_{f2} = -\frac{x_2}{3} + \frac{x_3}{6} + \frac{x_1}{6}, \\ \Delta\vec{y}_{f1} &= \frac{y_3}{3} - \frac{y_2}{6} - \frac{y_1}{6}, \qquad \Delta\vec{y}_{f2} = -\frac{y_2}{3} + \frac{y_3}{6} + \frac{y_1}{6}, \end{aligned} \tag{25}$$

TABLE 1: Comparison of the average Nusselt number Nu_{ave} for different grid resolutions at Ra = 10^5, Ha = 100, $r/L = 0.75$, and Pr = 0.025.

Mesh size						
31 × 91	41 × 121	51 × 151	61 × 181	71 × 211	81 × 241	91 × 271
2.1191	2.1485	2.1660	2.1781	2.1869	2.1937	2.1990

the derivatives of the shape functions are

$$N_{1x} = \frac{\partial N_1}{\partial x} = \frac{(y_2 - y_3)}{2V^{\text{ele}}}, \qquad N_{1y} = \frac{\partial N_1}{\partial y} = \frac{(x_3 - x_2)}{2V^{\text{ele}}},$$
$$N_{2x} = \frac{\partial N_2}{\partial x} = \frac{(y_3 - y_1)}{2V^{\text{ele}}}, \qquad N_{2y} = \frac{\partial N_1}{\partial y} = \frac{(x_1 - x_3)}{2V^{\text{ele}}},$$
$$N_{3x} = \frac{\partial N_2}{\partial x} = \frac{(y_1 - y_2)}{2V^{\text{ele}}}, \qquad N_{3y} = \frac{\partial N_3}{\partial y} = \frac{(x_2 - x_1)}{2V^{\text{ele}}}, \tag{26}$$

and the volume of the element is

$$V^{\text{ele}} = \frac{(x_2 y_3 - x_3 y_2) + x_1 (y_2 - y_3) + y_1 (x_3 - x_2)}{2}. \tag{27}$$

The obtained algebraic equations from the discretization procedure using CVFEM are solved by the Gauss-Seidel method.

Boundary conditions for the present problem can be applied using B_{B_i} and B_{C_i} as follows.

Insulated boundary:

$$B_{B_i} = 0, \qquad B_{C_i} = 0. \tag{28}$$

Insulated boundary:

$$B_{B_i} = 0, \qquad B_{C_i} = 0. \tag{29}$$

Fixed value boundary:

$$B_{B_i} = \phi_{\text{value}} \times 10^{16}, \qquad B_{C_i} = 10^{16}, \tag{30}$$

where ϕ_{value} is the prescribed value on the boundary. The volume source terms can be applied to (15) as

$$\sum_{j=1}^{\text{elements}} \int_{V_j} Q\, dV \approx Q_i V_i \tag{31}$$

or after linearizing the source term

$$Q_i V_i = -Q_{C_i} \phi_i + Q_{B_i}. \tag{32}$$

4. Grid Testing and Code Validation

A mesh testing procedure was conducted to guarantee the grid independency of the present solution. Various mesh combinations were explored for the case Ra = 10^5, Ha = 100, $r/L = 0.75$, and Pr = 0.025 as shown in Table 1. The present code was tested for grid independence by calculating the average Nusselt number on the inner circular wall. In harmony with this, it was found that a grid size of 81 × 241 ensures a grid-independent solution. The convergence criterion for the termination of all computations is

TABLE 2: Comparison of the present results with previous works for different Rayleigh numbers when Pr = 0.7.

Ra	Present	[36]	[37]
10^3	1.1432	1.118	1.118
10^4	2.2749	2.245	2.243
10^5	4.5199	4.522	4.519

$$\max_{\text{grid}} \left| \Gamma^{\hat{k}+1} - \Gamma^{\hat{k}} \right| \le 10^{-7}, \tag{33}$$

where $\hat{k}$ is the iteration number and Γ stands for the independent variables (Ω, Ψ, Θ). The present FORTRAN code is validated by comparing the obtained results for Pr = 0.7 with those reported in [36, 37] (see Table 2). Moreover, Table 3 shows the effects of a transverse magnetic field on natural-convection flow inside a rectangular enclosure which are compared with the results of Rudraiah et al. [15]. All of the previous comparisons indicate the accuracy of the present code.

5. Results and Discussion

In this study, natural convection heat transfer in an curved-shape enclosure in the presence of a magnetic field is investigated numerically using CVFEM. Calculations are made for various values of the Hartmann number, Ha = 0, 10, 100, and Rayleigh number, Ra = $10^3, 10^4, 10^5$.

Figures 3 and 4 show the isotherms and streamlines contours for different values of Rayleigh number and Hartmann number. At Ra = 10^3, the isotherms are parallel to each other and take the shape of the enclosure which are the main characteristics of conduction heat transfer mechanism. At Ra = 10^4, the circulation of the flow shows that the main eddy is divided into two eddies. Also, as Rayleigh number increases, the isotherms become more distorted and the stream function values are enhanced which is due to the domination of convective heat transfer mechanism at higher Rayleigh numbers. At this Rayleigh number, a thermal plume appears over the hot surface at $\gamma = 50^\circ$. At Ra = 10^5, one small counterclockwise eddy appears between two clockwise eddies. It is worthwhile mentioning that the effect of magnetic field is to decrease the value of the velocity magnitude throughout the enclosure because the presence of magnetic field introduces a force called the Lorentz force, which acts against the flow if the magnetic field is applied in the normal direction. This type of resisting force slows down the fluid velocity. Increasing Hartmann number has no significant

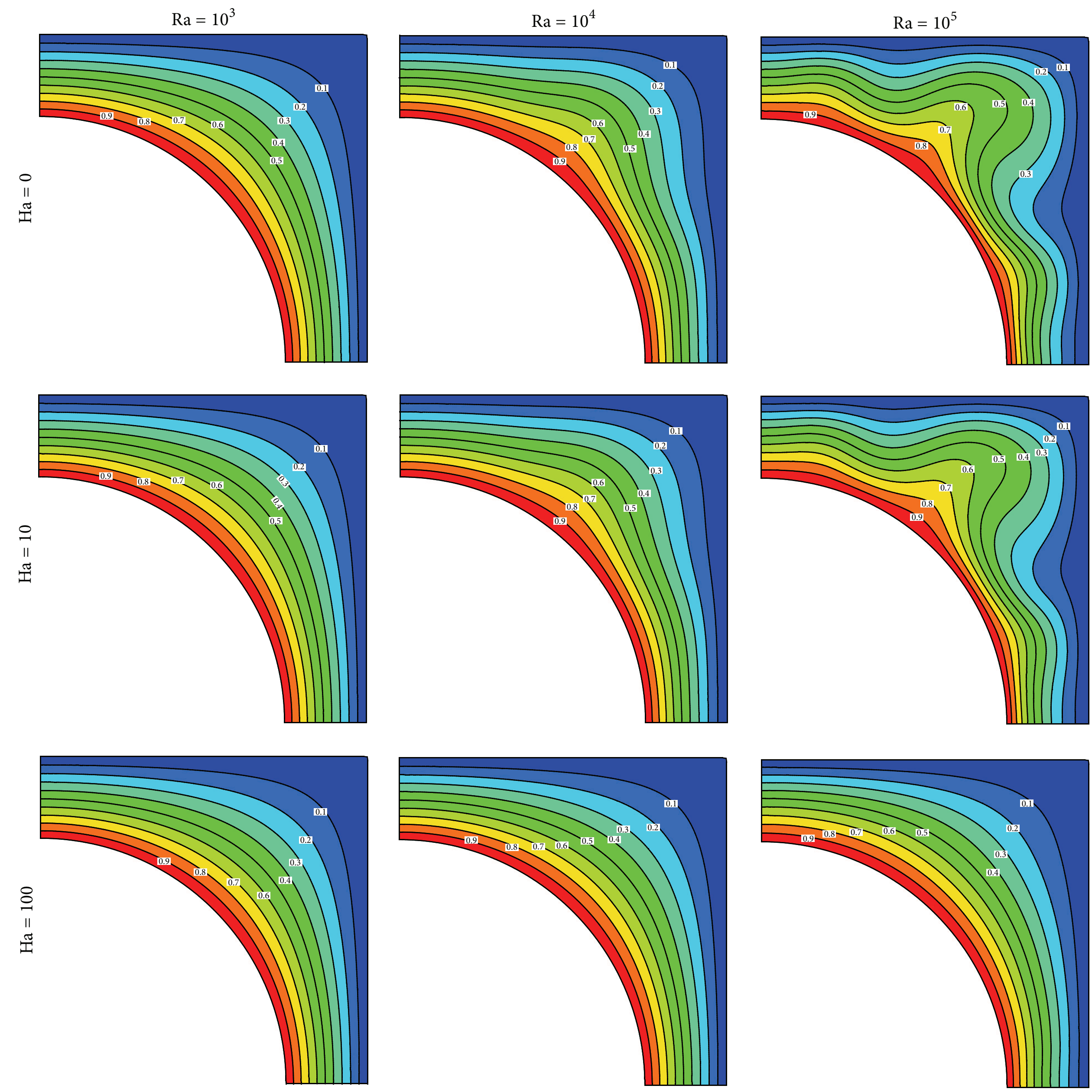

FIGURE 3: Isotherms contours for different values of Rayleigh number and Hartmann number at $r/L = 0.75$ and $\mathrm{Pr} = 0.025$.

effect on isotherms and streamlines at low Rayleigh number. At $\mathrm{Ra} = 10^4$, as Hartmann number increases, secondary eddies disappear and the core of voracity moves upward. At $\mathrm{Ra} = 10^5$, increasing Hartmann number up to $\mathrm{Ha} = 10$, two othercounter clockwise eddies appear. But in higher values of Hartmann number, it can be seen that all secondary eddies vanish. Also, it can be seen that in the presence of magnetic field, thermal plumes disappear.

Effects of the Rayleigh number and Hartmann number on local Nusselt number are shown in Figure 5. At $\mathrm{Ra} = 10^3$, the local Nusselt number profiles are symmetric with respect to $\gamma = 45^{\circ}$, which indicates the domination of conduction heat transfer mechanism. For higher Rayleigh number, local Nusselt number profiles are not symmetric and have extremums because of presence of thermal plumes. At $\mathrm{Ra} = 10^4$, in absence of magnetic field, the local Nusselt number profile has one local minimum at $\gamma = 50^{\circ}$. Increasing Hartmann number shifts this minimum point to $\gamma = 45^{\circ}$. At $\mathrm{Ra} = 10^5$, in the absence of magnetic field, the local Nusselt number profile has three local minima but as Hartmann number increases, these extrema disappear because of domination of conduction mechanism.

Figure 6 shows the effects of the Rayleigh number and Hartmann number on average Nusselt number and

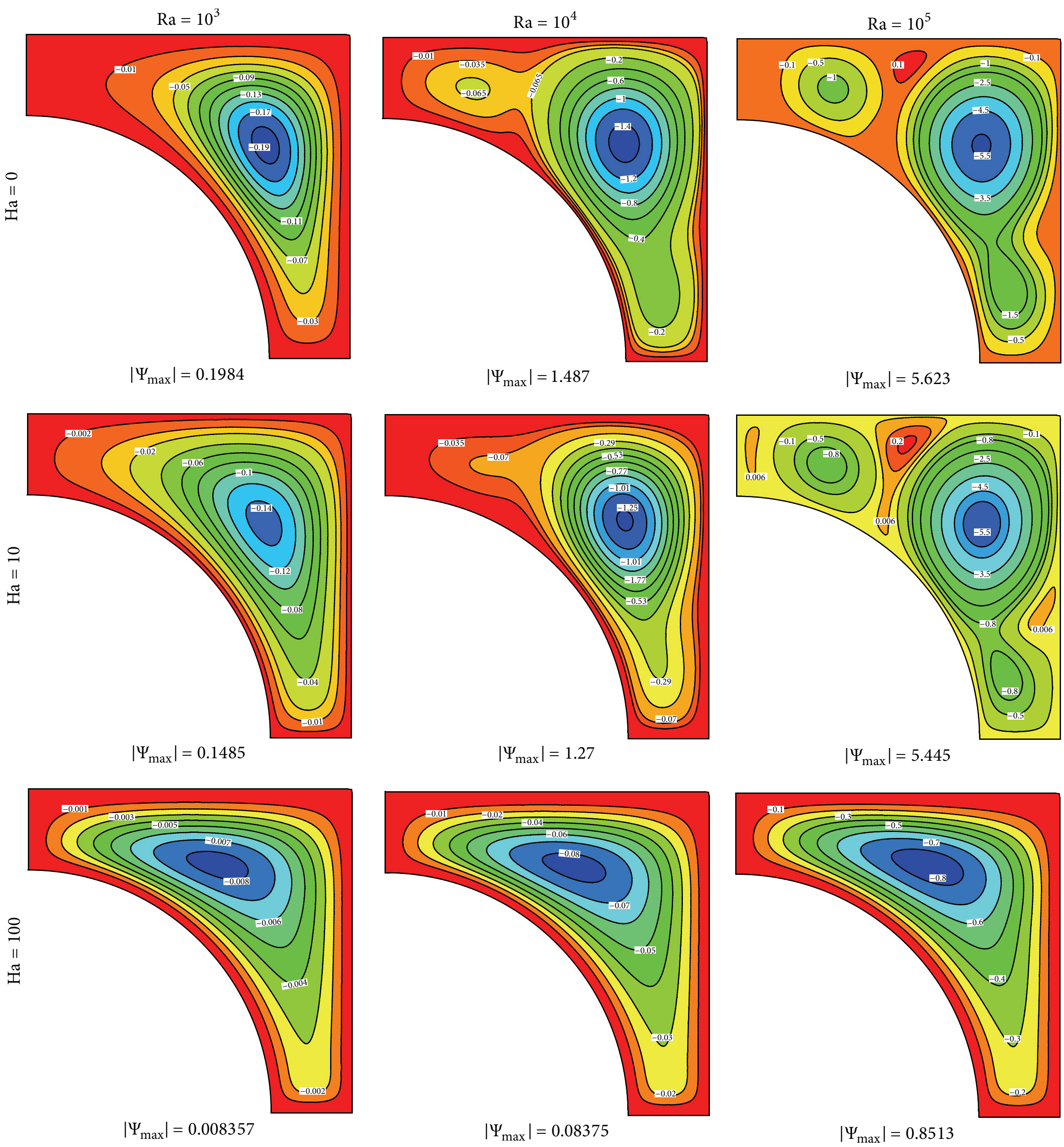

FIGURE 4: Streamlines contours for different values of Rayleigh number and Hartmann number at $r/L = 0.75$ and Pr = 0.025.

maximum value of stream function. As Rayleigh number increases, buoyancy force increases so that both thermal and velocity boundary layer thicknesses decrease. Increasing Rayleigh number leads to increase in average Nusselt number and $|\Psi_{max}|$. When the magnetic field is imposed on the enclosure, the velocity field is suppressed owing to the retarding effect of the Lorentz force. As Hartmann number increases boundary layer thicknesses increase, and in turn the average Nusselt number and $|\Psi_{max}|$ decrease.

TABLE 3: Average Nusselt number versus different Grashof numbers under various strengths of the magnetic field at Pr = 0.733.

Ha	Gr = 2×10^4		Gr = 2×10^5	
	Present	Rudraiah et al. [15]	Present	Rudraiah et al. [15]
0	2.5665	2.5188	5.093205	4.9198
10	2.26626	2.2234	4.9047	4.8053
50	1.09954	1.0856	2.67911	2.8442
100	1.02218	1.011	1.46048	1.4317

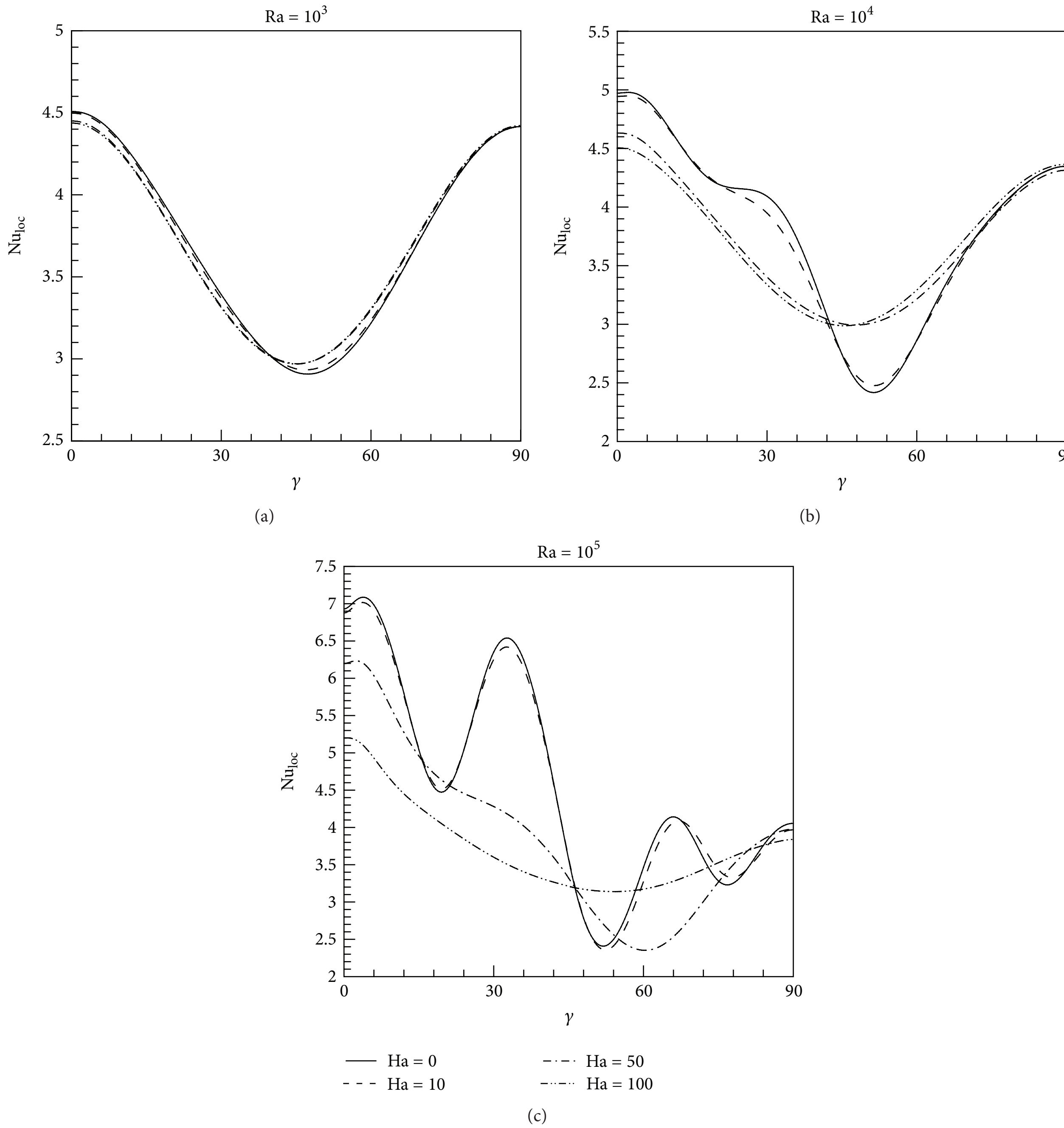

Figure 5: Effects of the Rayleigh number and Hartmann number on local Nusselt number.

6. Conclusion

In this study, natural convection heat transfer in a curved-shape inclined enclosure in the presence of magnetic field is investigated numerically using the control volume-based finite element method (CVFEM). From the numerical investigation, it can be concluded that the Hartmann number can be a control parameter for heat and fluid flow. In addition, it can be found that the Nusselt number and maximum value of stream function are increasing functions of Rayleigh number and decreasing functions of Hartmann number.

Nomenclature

C_p: Specific heat at constant pressure
Gr: Grashof number ($= g\beta\Delta TL^3/\upsilon^2$)
Ha: Hartmann number
Nu: Nusselt number
Pr: Prandtl number ($= \upsilon/\alpha$)
T: Fluid temperature
u, v: Velocity components in the x-direction and y-direction
U, V: Dimensionless velocity components in the X-direction and Y-direction

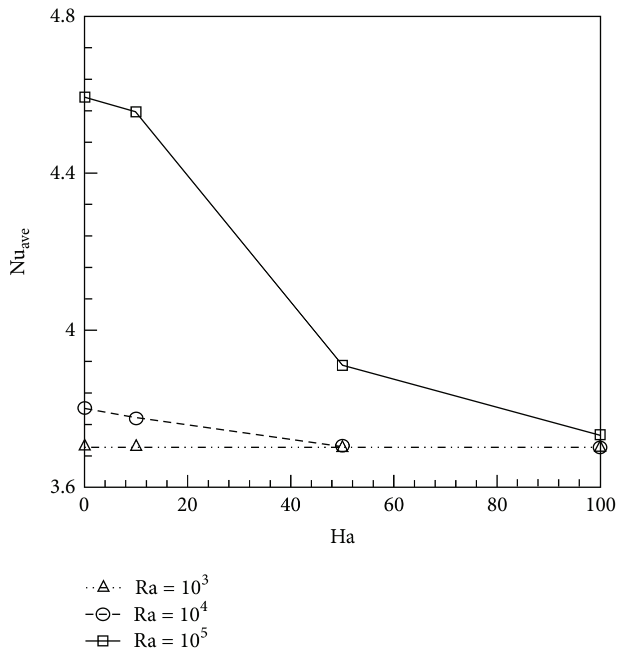

(a)

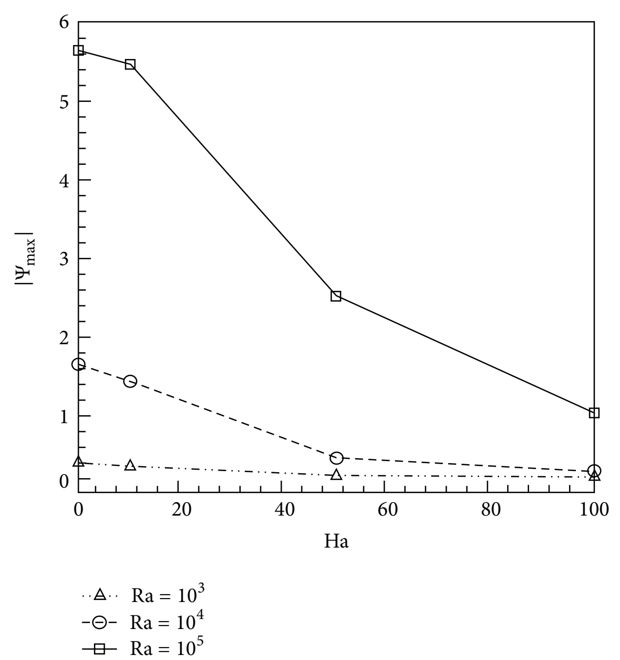

(b)

Figure 6: Effects of the Rayleigh number and Hartmann number on (a) average Nusselt number and (b) maximum value of stream function at $r/L = 0.75$ and $\mathrm{Pr} = 0.025$.

X, Y: Dimensionless space coordinates
r: Nondimensional radial distance
k: Thermal conductivity
L: Gap between inner and outer boundaries of the enclosure $L = r_{\text{out}} - r_{\text{in}}$
$\vec{g}$: Gravitational acceleration vector
Ra: Rayleigh number $(= g\beta\Delta T L^3/\alpha\nu)$.

Greek Symbols

ζ: Angle measured from the insulated right plane
α: Thermal diffusivity
σ: Electrical conductivity
μ: Dynamic viscosity
υ: Kinematic viscosity
ψ & Ψ: Stream function and dimensionless stream function
Θ: Dimensionless temperature
ρ: Fluid density
β: Thermal expansion coefficient.

Subscripts

c: Cold
h: Hot
loc: Local
ave: Average
in: Inner
out: Outer.

Acknowledgment

The authors thank the reviewers for comments which led to an improvement of the paper.

References

[1] H. A. Mohammed, A. Campo, and R. Saidur, "Experimental study of forced and free convective heat transfer in the thermal entry region of horizontal concentric annuli," *International Communications in Heat and Mass Transfer*, vol. 37, no. 7, pp. 739–747, 2010.

[2] T. H. Kuehn and R. J. Goldstein, "Correlating equations for natural convection heat transfer between horizontal circular cylinders," *International Journal of Heat and Mass Transfer*, vol. 19, no. 10, pp. 1127–1134, 1976.

[3] H. Bararnia, S. Soleimani, and D. D. Ganji, "Lattice Boltzmann simulation of natural convection around a horizontal elliptic cylinder inside a square enclosure," *International Communications in Heat and Mass Transfer*, vol. 38, no. 10, pp. 1436–1442, 2011.

[4] A. H. Srinivasa and A. T. Eswara, "Unsteady free convection flow and heat transfer from an isothermal truncated cone with variable viscosity," *International Journal of Heat and Mass Transfer*, vol. 57, no. 1, pp. 411–420, 2013.

[5] M. Sankar, Y. Park, J. M. Lopez, and Y. Do, "Numerical study of natural convection in a vertical porous annulus with discrete heating," *International Journal of Heat and Mass Transfer*, vol. 54, no. 7-8, pp. 1493–1505, 2011.

[6] K. Vajravelu, K. V. Prasad, R. A. Van Gorder, and J. Lee, "Free convection boundary layer flow past a vertical surface in a porous medium with temperature-dependent properties," *Transport in Porous Media*, vol. 90, no. 3, pp. 977–992, 2011.

[7] K. Khanafer, "Fluid-structure interaction analysis of non-Darcian effects on natural convection in a porous enclosure," *International Journal of Heat and Mass Transfer*, vol. 58, no. 1-2, pp. 382–394, 2013.

[8] C.-M. Fan, C.-S. Chien, H.-F. Chan, and C.-L. Chiu, "The local RBF collocation method for solving the double-diffusive natural convection in fluid-saturated porous media," *International Journal of Heat and Mass Transfer*, vol. 57, no. 2, pp. 500–503, 2013.

[9] F. T. Akyildiz, D. A. Siginer, K. Vajravelu, and R. A. Van Gorder, "Natural convection heat transfer of a viscous fluid in a vertical porous channel," *Journal of Engineering Mathematics*, vol. 74, no. 1, pp. 61–71, 2012.

[10] M. Sheikholeslami and D. D. Ganji, "Heat transfer of Cu-water nanofluid flow between parallel plates," *Powder Technology*, vol. 235, pp. 873–879, 2013.

[11] T.-Y. Na and I. Pop, "Free convection flow past a vertical flat plate embedded in a saturated porous medium," *International Journal of Engineering Science*, vol. 21, no. 5, pp. 517–526, 1983.

[12] M. Sheikholeslami, D. D. Ganji, and H. R. Ashorynejad, "Investigation of squeezing unsteady nanofluid flow using ADM," *Powder Technology*, vol. 239, pp. 259–265, 2013.

[13] M. Sheikholeslami, H. R. Ashorynejad, G. Domairry, and I. Hashim, "Flow and heat transfer of Cu-water nanofluid between a stretching sheet and a porous surface in a rotating system," *Journal of Applied Mathematics*, vol. 2012, Article ID 421320, 19 pages, 2012.

[14] S. C. Kakarantzas, I. E. Sarris, A. P. Grecos, and N. S. Vlachos, "Magnetohydrodynamic natural convection in a vertical cylindrical cavity with sinusoidal upper wall temperature," *International Journal of Heat and Mass Transfer*, vol. 52, no. 1-2, pp. 250–259, 2009.

[15] N. Rudraiah, R. M. Barron, M. Venkatachalappa, and C. K. Subbaraya, "Effect of a magnetic field on free convection in a rectangular enclosure," *International Journal of Engineering Science*, vol. 33, no. 8, pp. 1075–1084, 1995.

[16] M. Sheikholeslami, M. Gorji-Bandpay, and D. D. Ganji, "Magnetic field effects on natural convection around a horizontal circular cylinder inside a square enclosure filled with nanofluid," *International Communications in Heat and Mass Transfer*, vol. 39, no. 7, pp. 978–986, 2012.

[17] R. A. Van Gorder and K. Vajravelu, "Nonlinear hydro-magnetic convection at a permeable cylinder in a porous medium," *Heat and Mass Transfer*, vol. 47, no. 10, pp. 1323–1329, 2011.

[18] M. A. A. Hamad, I. Pop, and A. I. Md Ismail, "Magnetic field effects on free convection flow of a nanofluid past a vertical semi-infinite flat plate," *Nonlinear Analysis: Real World Applications*, vol. 12, no. 3, pp. 1338–1346, 2011.

[19] N. M. Al-Najem, K. M. Khanafer, and M. M. El-Refaee, "Numerical study of laminar natural convection in tilted enclosure with transverse magnetic field," *International Journal of Numerical Methods for Heat and Fluid Flow*, vol. 8, no. 6, pp. 651–672, 1998.

[20] T. Grosan, C. Revnic, I. Pop, and D. B. Ingham, "Magnetic field and internal heat generation effects on the free convection in a rectangular cavity filled with a porous medium," *International Journal of Heat and Mass Transfer*, vol. 52, no. 5-6, pp. 1525–1533, 2009.

[21] K. M. Khanafer and A. J. Chamkha, "Hydromagnetic natural convection from an inclined porous square enclosure with heat generation," *Numerical Heat Transfer A*, vol. 33, no. 8, pp. 891–910, 1998.

[22] M. A. Hossain, M. Z. Hafiz, and D. A. S. Rees, "Buoyancy and thermo capillary driven convection flow of an electrically conducting fluid in an enclosure with heat generation," *International Journal of Thermal Sciences*, vol. 44, no. 7, pp. 676–684, 2005.

[23] D. A. Nield, "Impracticality of MHD convection in a porous medium," *Transport in Porous Media*, vol. 73, no. 3, pp. 379–380, 2008.

[24] A. Barletta, S. Lazzari, E. Magyari, and I. Pop, "Mixed convection with heating effects in a vertical porous annulus with a radially varying magnetic field," *International Journal of Heat and Mass Transfer*, vol. 51, no. 25-26, pp. 5777–5784, 2008.

[25] H. R. Ashorynejad, M. Sheikholeslami, I. Pop, and D. D. Ganji, "Nanofluid flow and heat transfer due to a stretching cylinder in the presence of magnetic field," *Heat and Mass Transfer*, vol. 49, no. 3, pp. 427–436, 2013.

[26] H. R. Ashorynejad, A. A. Mohamad, and M. Sheikholeslami, "Magnetic field effects on natural convection flow of a nanofluid in a horizontal cylindrical annulus using Lattice Boltzmann method," *International Journal of Thermal Sciences*, vol. 64, pp. 240–250, 2013.

[27] M. Sheikholeslami, D. D. Ganji, H. R. Ashorynejad, and H. B. Rokni, "Analytical investigation of Jeffery-Hamel flow with high magnetic field and nano particle by Adomian decomposition method," *Applied Mathematics and Mechanics*, vol. 33, no. 1, pp. 25–36, 2012.

[28] M. Sheikholeslami, H. R. Ashorynejad, D. Domairry, and I. Hashim, "Investigation of the laminar viscous flow in a semi-porous channel in the presence of uniform magnetic field using Optimal Homotopy Asymptotic Method," *Sains Malaysiana*, vol. 41, no. 10, pp. 1281–1285, 2012.

[29] M. Sheikholeslami, H. R. Ashorynejad, A. Barari, and S. Soleimani, "Investigation of heat and mass transfer of rotating MHD viscous flow between a stretching sheet and a porous surface," *Engineering Computations*, vol. 30, no. 3, pp. 357–378, 2013.

[30] B. R. Baliga, "Control-volume finite element methods for fluid flow and heat transfer," in *Advances in Numerical Heat Transfer*, W. J. Minkowycz and E. M. Sparrow, Eds., vol. 1, Taylor & Francis, New York, NY, USA, 1996.

[31] V. R. Voller, *Basic Control Volume Finite Element Methods for Fluids and Solids*, World Scientific Publishing, 2009.

[32] S. Soleimani, M. Sheikholeslami, D. D. Ganji, and M. Gorji-Bandpay, "Natural convection heat transfer in a nanofluid filled semi-annulus enclosure," *International Communications in Heat and Mass Transfer*, vol. 39, no. 4, pp. 565–574, 2012.

[33] M. Sheikholeslami, S. Soleimani, M. Gorji-Bandpy, D. D. Ganji, and S. M. Seyyedi, "Natural convection of nanofluids in an enclosure between a circular and a sinusoidal cylinder in the presence of magnetic field," *International Communications in Heat and Mass Transfer*, vol. 39, no. 9, pp. 1435–1443, 2012.

[34] M. Sheikholeslami, M. Gorji-Bandpy, D. D. Ganji, and S. Soleimani, "Effect of a magnetic field on natural convection in an inclined half-annulus enclosure filled with Cu-water nanofluid using CVFEM," *Advanced Powder Technology*, 2013.

[35] M. Sheikholeslami, M. Gorji-Bandpy, D. D. Ganji, and S. Soleimani, "MHD natural convection in a nanofluid filled inclined enclosure with sinusoidal wall using CVFEM," *Neural Computing and Applications*, 2012.

[36] K. Khanafer, K. Vafai, and M. Lightstone, "Buoyancy-driven heat transfer enhancement in a two-dimensional enclosure utilizing nanofluids," *International Journal of Heat and Mass Transfer*, vol. 46, no. 19, pp. 3639–3653, 2003.

[37] G. De Vahl Davis, "Natural convection of air in a square cavity, a benchmark numerical solution," *International Journal for Numerical Methods in Fluids*, vol. 3, no. 3, pp. 249–264, 1962.